Applied Nanoscience (2019) 9:1037–1045
https://doi.org/10.1007/s13204-018-0749-1

ORIGINAL ARTICLE

Structural characteristics and sorption properties of lithium-selective composite materials based on TiO_2 and MnO_2

M. O. Chaban[1] · L. M. Rozhdestvenska[1] · O. V. Palchyk[1] · Y. S. Dzyazko[1] · O. G. Dzyazko[2]

Received: 5 January 2018 / Accepted: 26 March 2018 / Published online: 4 April 2018

Abstract

A number of nanomaterials containing titanium dioxide and manganese dioxide were synthesized. The effect of synthesis conditions on structural and sorption characteristics for the selective extraction of lithium ions from solutions was studied. The ion-exchange materials were investigated with the methods of electron microscopy, thermogravimetric and X-ray analyses. During thermal synthesis phases of lithium manganese titanium spinel and TiO_2 are being formed. Replacing a part of manganese with titanium ions leads to a decrease in the dissolution of Mn and to an increase in chemical stability. Composites with optimal values of selectivity and sorption rates were used to remove lithium ions from solutions with high salt background. The recovery degree of lithium ions under dynamic conditions reached 99%, the highest sorption capacity was found at pH 10.

Keywords Nanoparticles · Titanium dioxide · Manganese dioxide · Lithium · Sorption

Background

Lithium consumption has strong growing demand due to wide lithium application in Li-ion rechargeable batteries, glass, ceramics, grease, nuclear fusion fuel, metallurgical industries, light aircraft alloys, pharmaceuticals (Heidari and Momeni 2017). Solar evaporation, solvent extraction, co-precipitation (using aluminum salt), membrane processes, liquid–liquid extraction—these methods are used for lithium recovery from mines, brines, and salt lakes (Hamzaoui et al. 2003; Epstein et al. 1981; An et al. 2012; Swain 2016; Gao et al. 2016).

Such alternative resources as seawater and secondary waste solutions also should be used. However, the content of this element in seawater is rather small (0.17 mg/l). Among metal ions, Li^+ species are characterized by the smallest radius (7.8×10^{-11} m), increased polarization ability and tendency to solvation. This and also high concentration of other inorganic ions (Na^+, Ca^{2+}, Mg^{2+}, etc.) complicate Li^+ sorption. Thus, development of highly selective materials is very important task.

Adsorption and ion exchange are the most preferable techniques for recovery of inorganic ions from very diluted solutions, inorganic sorbents are very effective for this purpose (Alberti and Massucci 1970). A number of inorganic materials has been proposed, for instance, titanium antimonate (Abe and Chitrakar 1987).

Among inorganic materials, hydrated oxides of multivalent metals are attractive as sorbents of various inorganic ions due to simple synthesis techniques, which requires cheap raw material, high selectivity, particularly towards Li^+ (Kim et al. 2008), and possibility to sorb both cations and anions depending on the solution pH (Amphlett 1964; Kudelko et al. 201111). Due to these remarkable properties, oxide materials are used not only as sorbents, but also as modifiers for ceramic (Dzyazko et al. 2006, 2014a, b; Marti-Calatayud et al. 2015; Mora-Gómez et al. 2017) and polymer membranes (Hong et al. 2015; Dzyazko et al. 2017) for electrodialysis, as well as for development of the membranes applied to filtration affected by pressure gradient (Huang et al. 2012; Pang et al. 2014; Myronchuk et al. 2016). Particles of oxides of multivalent metals, which are precipitated in inert polymers (Myronchuk et al. 2016), are smaller than formations of phosphate compounds (Dzyazko et al. 2015,

✉ M. O. Chaban
mary.chaban@gmail.com

[1] V.I. Vernadskii Institute of General and Inorganic Chemistry of National Academy of Sciences of Ukraine, 32/34 Paladin Ave., Kiev 03142, Ukraine

[2] Taras Shevchenko National University of Kyiv, 64/13, Volodymyrska Str., Kiev 01601, Ukraine

Myronchuk et al. 2016). Calcination of hydrated oxides such as MnO_2 (Ooi et al. 1986; Park et al. 2015) or TiO_2 (Chitrakar et al. 2014; Shi et al. 2013; Tretyak et al. 2013; Zhang et al. 2010) allows one to obtain Li-selective sorbents.

Spinel-type lithium–manganese oxides (LMO, their composition is $Li_nMn_{2-x}O_4$, where $1 \le n \le 1.33$, $0 \le x \le 0.33$) were found to be the most attractive materials for preparation of highly selective sorbents, which can be obtained by means of $Li^+ \rightarrow H^+$ exchange (Ooi et al. 1986; Park et al. 2015). With increasing ratio of Li/Mn, higher values of sorption capacity are achieved. However, regeneration with acidic solutions destroys these oxides due to reaction of disproportionation of Mn(III) followed by removal of Mn(II) from the solid.

Other types of lithium-ion sieves were proposed: H_2TiO_3 with a layered structure and $H_4Ti_5O_{12}$ with a spinel structure. These compounds (LTO) are characterized by a higher stability due to large energy of titanium–oxygen bond (Chitrakar et al. 2014; Shi et al. 2013; Zhang et al. 2010). Selectivity is formed by means of saturation of the initial amorphous titanium dioxide with Li^+ cations followed by thermal treatment (Tretyak et al. 2013).

In order to provide high sorption rate, small grains of the Li-selective sorbent are attached to the binder (Umeno et al. 2002; Hong et al. 2013; Chung et al. 2014; Xiao et al. 2015; Hong and Chen 2015; Kam et al. 2015), in this case lower sorption capacity is reached (Chung et al. 2017). Other approach is to obtain LMO nanoparticles (Miyamoto et al. 2015). In this case, the limiting stage of sorption is diffusion through grains. Regarding the materials containing large primary particles, sorption rate is determined by chemical reaction (Li^+ insertion to spinel structure). Multiple processes of sorption-regeneration result in destruction of the sorbents.

Double hydrated oxides containing MnO_2 possess higher selectivity towards Li^+ comparing with oxides based on one metal (Hong et al. 2018). Regarding sorption of heavy metal cations, this is explained by high microporosity of manganese oxide, since micropores are considered as selective sorption centers (Mal'tseva et al. 2011). Calcination of oxides of complex composition containing two or even more multivalent metals allows one to obtain lithium conductors (Bohnke 2008). The materials of this type were applied to preparation of Li-selective membrane for recovery of this element from sea water using reverse electrodialysis (Hoshino 2015). However, mechanical durability of the membranes is expected to be rather low.

Double titanium–manganese oxide (LTMO) possesses selectivity towards Li^+ (Jiang 2012). This sorbent was obtained by using a method of solid-state reaction, the grains consisted of coarse particles. The aim of the investigation was to obtain and test the nanomaterial of similar composition. As expected, the nanosized particles would provide high sorption rate.

Experimental

Synthesis of LTMO and LTO

Synthesis of titanium–manganese sorbents was carried out through redox reaction between $TiCl_4$ and $KMnO_4$ solutions. The concentration of each solution was 1 M, their volumes were equal. An excess of HCl, which is formed during $TiCl_4$ hydrolysis, provides Mn(VII) → Mn(II) transformation:

$$TiCl_4 + 2H_2O \rightarrow TiO_2 + 4HCl \quad (1)$$

$$2KMnO_4 + 16HCl \rightarrow 2MnCl_2 + 2KCl + 8H_2O + 5Cl_2. \quad (2)$$

Further disproportionation reaction occurs:

$$4KMnO_4 + 3MnCl_2 + 4HCl \rightarrow 7MnO_2 + 4KCl + 2H_2O + 3Cl_2 \quad (3)$$

The resulting reaction:

$$2TiCl_4 + 2KMnO_4 + 2H_2O \rightarrow 2TiO_2 + 2MnO_2 + 2KCl + 2H_2O + 3Cl_2 \quad (4)$$

Gel consisting of Ti and Mn hydrated dioxides is obtained by this manner. Poor solubility of $KMnO_4$ in water when added to the $TiCl_4$ solution provides control over the rate of neutralization of excess acidity, slowing down the process of gel formation. Optimal conditions for the formation of the double oxide are achieved by this manner.

The obtained hydrogel was washed with distilled water until MnO_4^- and Mn^{2+} were absent in the effluent, then it was dried under room temperature. The inorganic material was in the form of durable black granules of irregular shape. The grains were washed with 12% aqueous ammonia solution and distilled water, then were dried again.

A 1 M $TiCl_4$ solution containing equimolar amount of citric acid was used to synthesize hydrated titanium dioxide. Gel was precipitated with 10% NH_4OH solution and dried at room temperature.

The granular sorbents (hydrated oxides of both Ti and Ti–Mn) were loaded with lithium by treatment with a 1 M LiOH solution for 48 h. A volume ratio of sorbent and solution was 1:100. Further the sorbent was separated from the solution, washed with distilled water and dried in air at room temperature down to constant mass. The lithiated form of the samples was calcinated at 500, 600 and 700 °C for 4 h. To remove Li^+ ions (provide $Li^+ \rightarrow H^+$ exchange), the samples were washed with 0.5 M HCl and analyzed with an atomic absorption method using a PYE UNICAM SP 9 spectrometer (Philips).

Characterization of the samples

For chemical analysis, the samples of the obtained materials were analyzed with an X-ray fluorescent spectrometer X-Supreme 8000 XRF (Oxford Instruments).

Microphotographs were obtained by using a Trek DCM510 camera with a RL05-48 ring diode illuminator attached to a PZO optical microscope (PZO, Poland).

TEM images of granules were obtained by using a transmission microscope JEOL JEM 1230 (JEOL, Japan). Scanning Electron Microscope Tescan Mira 3 LMU (Czech Republic) was also applied to the research.

Differential thermal analyses were carried out in the range of 20–800 °C at a scanning rate of 5 °C/min («Derivatograph Q - 1500 D», Paulik-Paulik-Erday, Hungary). For X-ray analysis, a diffractometer DRON-3M (LOMO, Russia) with external standards certified by SiO_2 (standard 2θ) and Al_2O_3 (intensity standard) was used (Cu-radiation, Ni-filter) (Nat Inst of Standards and Technology 1991). Isotherms of nitrogen adsorption–desorption were obtained with an automatic gas adsorption analyzer of surface and porosity Quantachrome AS1Win (Quantachrome Instruments, USA). The specific surface area was estimated from the isotherms with the BET method, the total volume of micro- and mesopores was determined with the BJH method (Gregg and Sing 1982).

Testing of the samples

Preliminarily fraction of 0.16–0.25 mm was taken for study of sorption under dynamic conditions in a column. A diameter of the column was 0.6 cm, the height of the sorbent bed was 17 cm. The recovery of Li^+ ions was carried out from the solution containing 1×10^{-4} M LiCl. Superficial flow velocity was 0.18 m/h or one volume of the sorbents bed (BV) per hour. Li^+ content at the column outlet was analyzed, sorption capacity was calculated as pointed in Helfferich (1995).

Further sorption from the solution containing 0.1 M LiCl, 0.5 M NaCl and also NH_4OH-NH_4Cl buffer (the initial pH values were 8, 10 and 12) was investigated under batch conditions. The solution containing LiOH (0.1 M) and NaCl (0.5 M) was also used, the initial pH was about 10. The mass ratio of sorbent:solution was 0.01:50, the time of contact was 24 h. The pH of the equilibrium solution was determined using the I-160NI ionomer (Analitprylad, Ukraine). The distribution coefficients (K_d) and selectivity coefficients (K_s) were determined as $K_d = \bar{C}_{Li}/C_{Li}$ and $K_s = \bar{C}_{Li}C_{Na}/(C_{Li}\bar{C}_{Na})$, where C and $\bar{C}$ are the concentration of ions in the solution and ion exchanger (Helfferich 1995).

Results

Morphology of grains: thermogravimetric analysis

The synthesized titanium–manganese sorbent is in a form of shiny granules with average size of 0.25–0.5 mm (Fig. 1a). Shape of the grains is close to that of titanium dioxide (Fig. 1b).

Crystallization of the oxyhydrate matrix occurs during the thermal treatment, which provides mechanical durability of the grains. This procedure is accompanied by shrinkage and compaction of the material. According to the TG–DTA analysis, one or two clear endothermic effects and several exothermic effects are recorded in the high-temperature range (Table 1). Thus, the endothermic peak at 100–250 °C is related to the removal of weakly bonded water, which causes the main mass loss. The second endopeak corresponding to condensation of OH groups is observed only for lithium-substituted titanium oxide (TiO_2–Li). In this case, Ti–O–Mn and Ti–O–Ti bonds

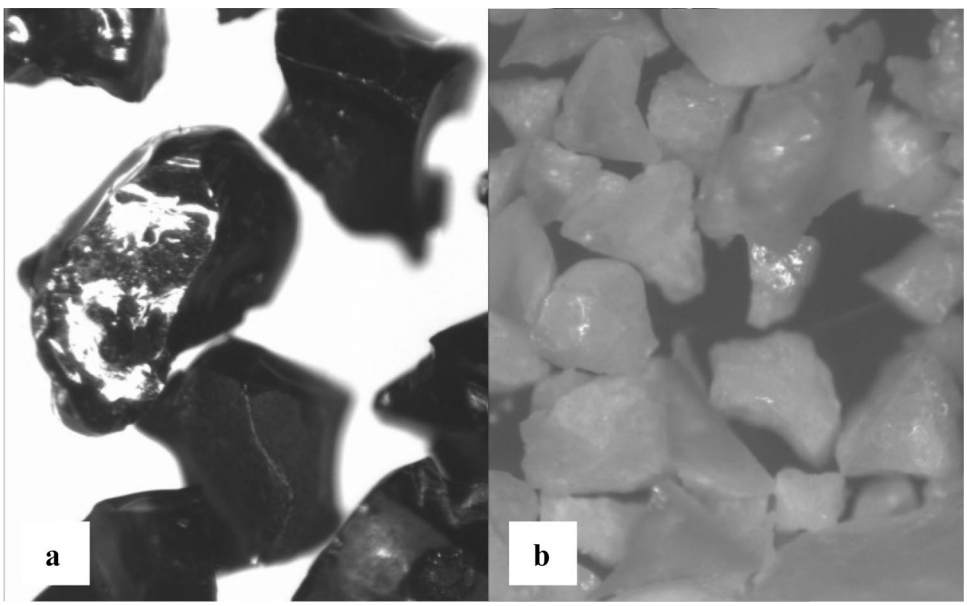

Fig. 1 Images of the sorbents: LTMO (**a**) and LTO (**b**)

are formed. In the temperature range of 300–500 °C, overlapping of thermal effects occurs due to removal of water from different structural positions. In the range of growth of the exothermic effect (250–650 °C), the mass loss is insignificant, several small exopeaks are recorded. They are related to crystallization of the amorphous phase and polymorphic transformations. Thus, spinel structure is formed above 500–600 °C. This assumption can be confirmed by the data from an X-ray diffraction analysis.

X-ray analysis

In the temperature range of the first and second endoeffects (100–400 °C), the samples are amorphous. In the case of titanium dioxide anatase structure is formed at 400–500 °C, this phase is transformed into rutile above 700 °C (Diebold 2003). The data of X-ray diffraction analysis for the LTO sample show crystalline structure above 500 °C (Fig. 2). The sample, which was calcinated at 500 °C, consists of anatase (76.4%) and lithium titanium spinel $LiTi_2O_4$ (23.6%) (Table 2). Regarding spinel phase, its space group is *Fd*3*m*, $a = 8.25$ Å, cell volume is 561.61 Å^3. With an increase in the calcination temperature up to 700 °C, the content of anatase reduces (decrease in the intensity of its X-ray reflexes). At the same time, intensity of the reflexes corresponding to rutile and $Li_4Ti_5O_{12}$ (the space group is *Fd*3*m*, $a = 8.35$ Å, cell volume is 583 Å^3) increases. Therefore, the composition of LTO depends on thermal treatment conditions. $Li_4Ti_5O_{12}$ phase is formed at 700 °C. A mixture of crystalline structures of lithium titanate, anatase and rutile is formed in the region of lower temperature.

Table 1 Data of thermogravimetric studies

Peaks	Sample	LTO	LTMO
1st endopeak	Range (°C)	170–318	148–360
	T_{max}	238	230
	Δm (%)	3.2	8.0
2nd endopeak	Range (°C)	380–490	–
	T_{max}	405	–
	Δm (%)	6.5	–
3rd exopeak	Range (°C)	590–720	560–760
	T_{max}	628, 661, 719	625, 678, 710
	Δm (%)	–	
Δm (%)		9.7	8.0

A size of regions of coherent scattering was calculated from the half-width of reflexes using Scherrer formula (Scherrer 1918):

$$D = \frac{K\lambda}{(\Delta^2 - \Delta_0^2)^{0.5}\cos\theta}, \tag{5}$$

where $K = 2\sqrt{\frac{\ln 2}{\pi}} \approx 0.9$. Here D is the crystallite size, λ is the wave length, Δ is the width of reflex at its half-height, Δ_0 is the similar parameter, which is caused by the apparatus (this value is determined using LaB_6 standard), and θ is the

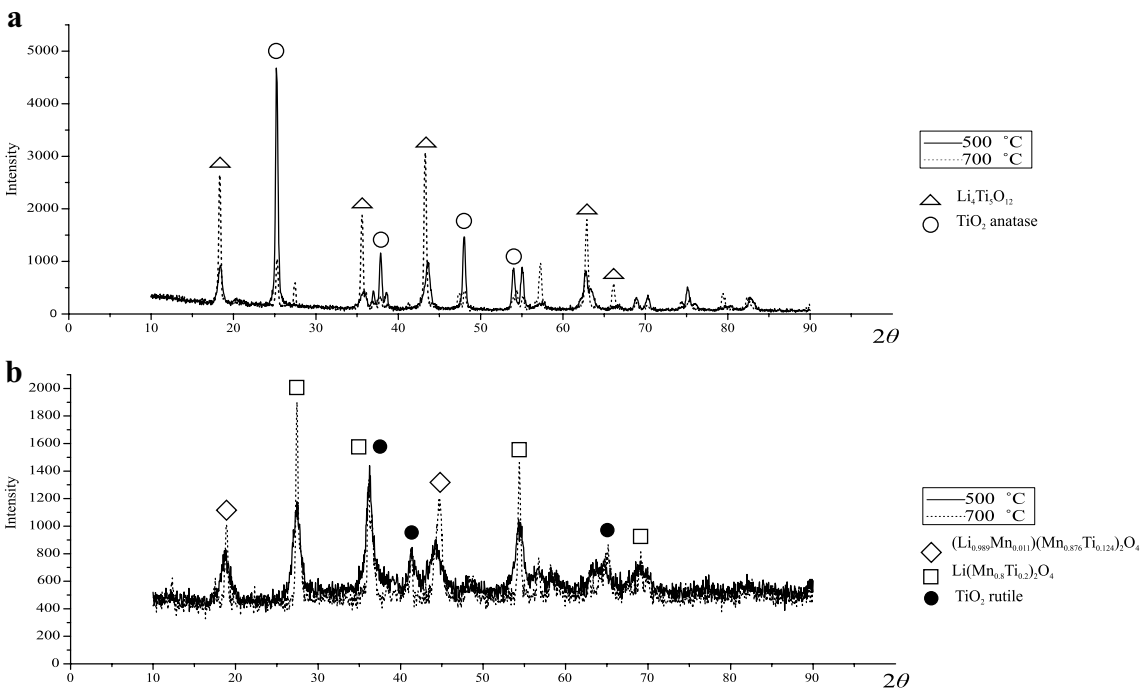

Fig. 2 X-ray pattern of TiO_2-Li (**a**) and TiO_2–MnO_2–Li (**b**) obtained at 500 and 700 °C

Table 2 Phase composition

Sample	Calcination temperature (°C)	Phases	Average size of primary particles (nm)
LTO	500	Anatase, 76.4%	17.7
		$LiTi_2O_4$ spinel, 23.6%	18
LTMO	500	Rutile, 49.1%	11.5
		MnO_2, 50.9%	19.5
LTO	700	Anatase, 32%	20
		Rutile, 46.2%	20
		$Li_4Ti_5O_{12}$, 21.8%	9
LTMO	700	Rutile, 59.3%	34
		$Li_{0.75}Mn_{0.25}Ti_2O_4$ spinel, 40.7%	26.7

angle corresponding to the reflex maximum. The data are given in Table 2.

In the case of LTMO, $Li_{0.75}Mn_{0.25}Ti_2O_4$ spinel is formed at 500 °C (its space group is *Fd*3*m*, $a = 8.46$ Å, cell volume is 654 $Å^3$) (Lambert et al. 1988). This phase coexists with $LiMn_2O_4$ and rutile. With increasing temperature of calcination up to 700 °C, the largest reflexes correspond to the rutile and titanium–manganese spinel enriched with manganese $Li(Mn_{0.8}Ti_{0.2})_2O_4$ (space group *Fd*3*m*, $a = 8.28$ Å, cell volume is 569 $Å^3$) (Cho et al. 1997).

Visualization of nanoparticles and their aggregates

For example, TEM images for the LTMO sample calcinated at 700 °C are given in Fig. 3. The materials are composites, since the image contains no contrast spots, which is confirmed by the data of X-ray analysis. Sizes of primary particles are about 15–40 nm and they form aggregates with size of 50–400 nm, as seen from SEM image (Fig. 4). Smaller aggregates are formed at lower temperature (up to 250 nm); and in this case, the aggregates are more compact.

Pores and specific surface area

Packing of the sorbent structure with increasing calcination temperature is also confirmed by data of porosity measurements (Table 3). Fraction of micropores in pore volume, which includes micro- and mesopores (the method of capillary condensation, i.e., nitrogen adsorption technique allows us to determine only these types of pores), decreases under elevated temperature. The size of dominant pores shifts toward larger radii indicating merger of the primary particles. The rise in processing temperature over 500 °C is accompanied by a sharp decrease in the pore volume due to shrinkage and compaction of the particles. The method of capillary condensation gives an estimate of the general structural characteristics of the sorbent, but does not reflect the data of lithium-selective sorption centers, a size of which corresponds to Li^+ ions. This information could be obtained only from sorption experiments.

Li^+ sorption under batch and dynamic conditions

From the calculated selectivity coefficients $K_{Li/Na}$ and distribution coefficients $K_{d_{Li}}$ (Table 4), it can be seen that the lithium distribution coefficients for sorption materials

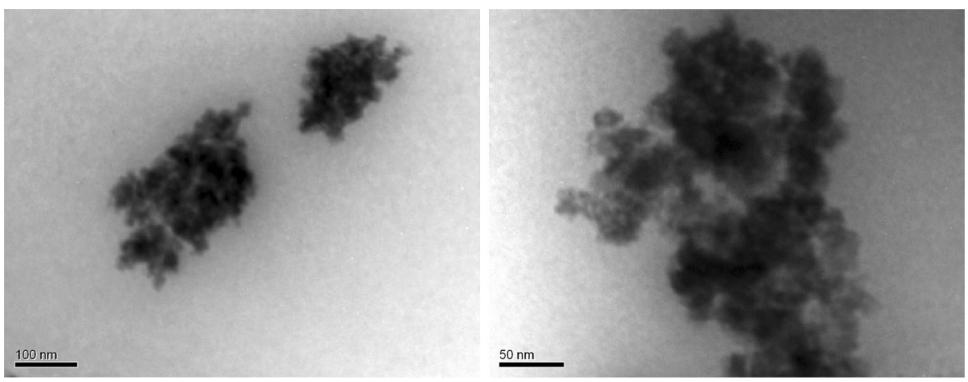

Fig. 3 TEM picture of the LTMO sample calcinated at 600 °C

containing manganese are higher than for titanium dioxide; and binary materials are generally more selective to lithium. In addition, the decrease of $K_{d_{Li}}$ values with transition to higher temperatures of synthesis is worth noting, which is explained by structural transformations in the material at 700 °C. As for the dependence of the selectivity factors on the pH of the adsorbate solution, it can be noted that there is no clear correlation for binary materials. However, there is a difference in the selectivity between sorption from buffer and non-buffer solutions that is explained by the competition between sodium and ammonium ions, as a result of which the sodium sorption is reduced and $K_{Li/Na}$, respectively, increases.

Figure 5 illustrates concentration of Li^+ ions at the column outlet relatively to the initial concentration as a function of bed volume (a ratio of volumes of the passed solution and

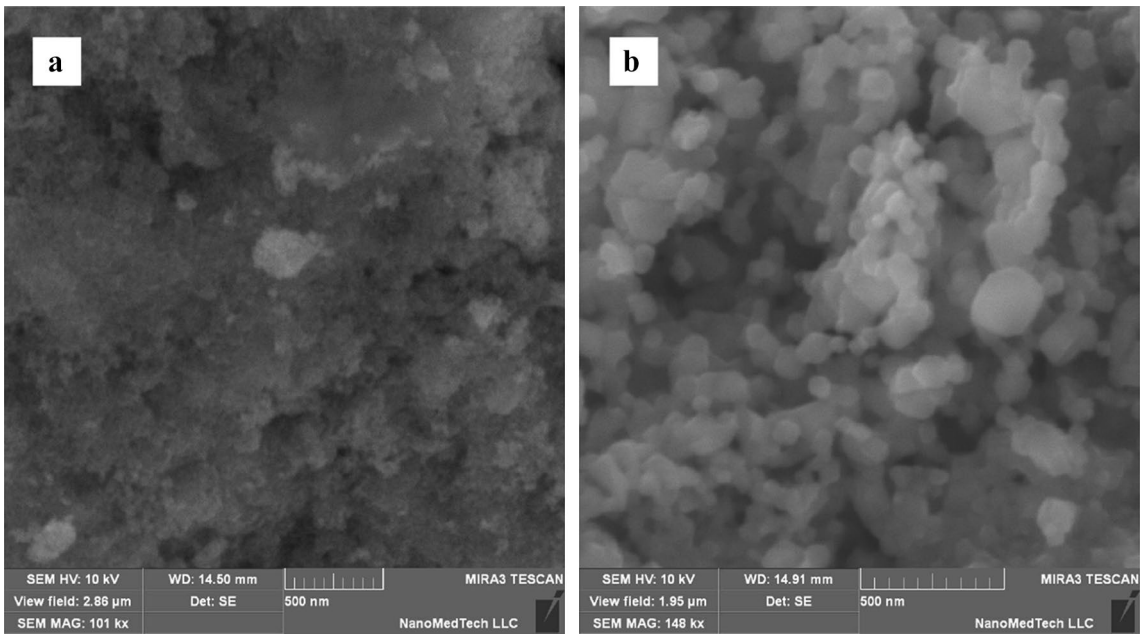

Fig. 4 SEM images of the LTMO sorbent calcined at 500 °C (**a**) and 700 °C (**b**)

Table 3 Structural characteristics of the synthesized materials

Parameters	TiO_2			TiO_2–MnO_2		
Calcination temperature (°C)	400	500	600	400	500	600
Surface area (m^2/g)	125.7	95.8	9.03	125.9	121.9	86.4
Total volume of micro- and mesopores (cm^3/g)	0.147	0.125	0.023	0.282	0.299	0.223
Fraction of micropores (%)	14.3	14.4	5.1	24.9	19.7	18.8
Average pore radius (A)	37.33	40.13	96.44	27.5	34.8	35.96

Table 4 Selectivity coefficients $K_{Li/Na}$ and distribution coefficients $K_{d_{Li}}$ obtained under batch conditions

Sample	T (°C)	$K_{d_{Li}}$				$K_{Li/Na}$			
		pH 8	pH 10	pH 12	pH 10*	pH 8	pH 10	pH 12	pH 10[a]
LTO	500	11.5	25.2	34.4	64.9	2.8	4.2	9.0	58.4
	600	72.7	96.9	74.9	105.9	23.7	25.3	30.2	516.4
	700	13.8	6.8	8.9	11.1	112.2	211.6	84.2	4.8
LTMO	500	216.1	85.2	94.1	124.2	40.0	123.5	128	123
	600	180.9	61.4	126.8	98.1	684.5	147.7	224	3.5
	700	136.4	60.0	68.1	86.1	990.3	146.3	225	4.2

[a]pH 10—the solution was free from ammonia buffer

sorbent). The data are given for the LTMO sample calcinated at 700 °C. It is shown that when passing about 150 bed volumes of the solution, the degree of lithium recovery reached 99%. The ion exchanger retention time was 78 h. The breakthrough capacity, at which rapid decrease of the curve is observed, is about 0.27 mmol/g, i.e., ≈ 10% of the maximum value under the given experimental conditions. Micropore filling is fast and does not significantly affect sorption rate. The synthesized composites are mainly mesoporous, diffusion is proportional to the concentration gradient. Under these conditions, the rate of sorption is determined by availability of selective sorption centers. Before the break-through capacity, sorption rate is 3.71×10^{-10} mol/(g s), its lower by 1–2 order of magnitude comparing with sorption of transition metals on ion exchange resins (Dzyazko et al. 2006).

Regarding other samples, no Li^+ removal under dynamical conditions was found despite rather high distribution coefficients obtained under batch conditions (Table 4). It means very slow sorption by the samples, which are free from manganese. This is also valid for the LTMO sample calcinated at 500 °C. As shown for inorganic ion-exchangers (zirconium hydrophosphate), increase of sorption capacity slows down sorption (Dzyazko et al. 2006). Indeed, among LTMO sorbents, the lowest distribution coefficients were found for the sample calcinated at 700 °C.

It was found that the LTMO sorbents show high selectivity towards Li^+ ions during sorption from the solution containing also Na^+ and NH_4^+. The best selectivity is reached at pH 10. Decrease of the pH results in deterioration of sorption evidently due to decrease of surface charge density, since oxide materials are amphoteric (Amphlett 1964). Indeed, ion exchange mechanism makes sufficient contribution to sorption (the values of equilibrium pH are ≈ 4).

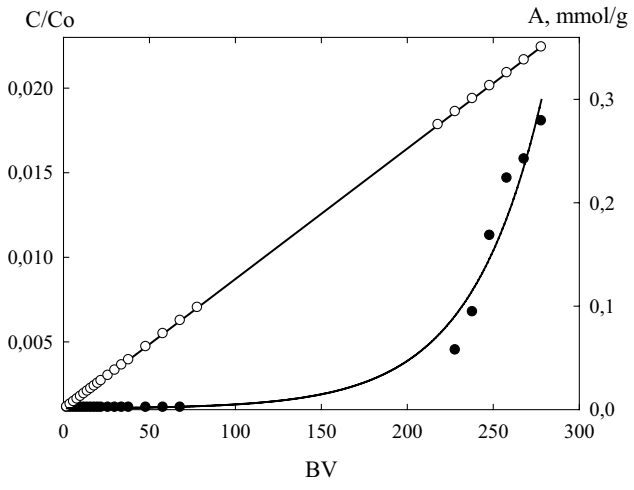

Fig. 5 Concentration of Li^+ ions at the column outlet relatively to the initial concentration (dark symbols) and sorption capacity (white symbols) as functions of bed volume

Cation exchange ability of the samples enhances in alkaline solutions. However, lower distribution and selectivity coefficients were obtained at pH 12. This is caused by competition between Li^+, Na^+, and NH_4^+ ions. This assumption is confirmed by the data obtained for the solution containing no ammonia buffer. In this case, higher distribution and selectivity coefficients were found than those for the solution containing the buffer.

Discussion

The LTMO sample containing nanosized particles of rutile and nanosized $Li_{0.75}Mn_{0.25}Ti_2O_4$ spinel provides sufficient Li^+ uptake probably due to formation of selectivity centers. These centers are evidently formed during synthesis, when Li-loaded forms of hydrated double oxide being calcinated followed by partial Li^+ removal. Nanosized particles provide sufficient sorption rate, this allows us to remove Li^+ ions from aqueous solutions under dynamic conditions. The material demonstrates preferable sorption of Li^+ ions over Na^+ and NH_4^+. Since sorption is rather slow (very low feed velocity is needed), it is necessary to use large volume of the sorbent to achieve the most complete lithium recovery. Other way is grinding the sorbent and use combining method of sorption and microfiltration similar to Zhang et al. (2009). This problem will be investigated in future.

Conclusions

LTO and LTMO nanomaterials were obtained by loading of hydrated oxides with Li^+ ions, calcination followed by removal of lithium from the solid. The sorbents are related to nanomaterials; this evidently facilitates sorption. Increase of calcination degree up to 700 °C results in insufficient enlargement of the nanoparticles. At the same time, the grains become larger and their packing are looser. In the case of LTMO containing rutile, anatase and $Li_{0.75}Mn_{0.25}Ti_2O_4$ spinel, nanodimensional particles make it possible to remove Li^+ ions from aqueous solutions under dynamic conditions. These sorbents show the highest Li^+ sorption, when these ions are recovered from multicomponent solutions. This is evidently due to formation of selective sorption centers. The highest sorption capacity was found to be reached at pH 10, and ion exchange mechanism makes its contribution to sorption. Due to rather low sorption rate, the material could be recommended as a modifier to prepare Li^+-selective membranes. In order to accelerate sorption, it is recommended to obtain smaller grains and attach them to porous support.

Acknowledgements The work was supported by projects within the framework of programs supported by the National Academy of Science

of Ukraine "Fundamental problems of creation of new materials for chemical industry" (Grant No. 49/12).

Author contributions MC investigated sorption properties of the materials and prepared the manuscript; LR provided porosimetric and thermogravimetric measurements; PO synthesized the samples; YD studied chemical composition and morphology of the samples; OD provided X-ray analysis.

Compliance with ethical standards

Conflict of Interest The authors declare that they have no competing interests.

References

Abe M, Chitrakar R (1987) Synthetic inorganic ion-exchange materials. XLV. Recovery of lithium from seawater and hydrothermal water by titanium (iv) antimonate cation exchanger. Hydrometallurgy 19(1):117–128

Alberti G, Massucci M (1970) Crystalline insoluble acid salts of tetravalent metals—IX. J Inorg Nucl Chem 32(5):1719–1727

Amphlett CB (1964) Inorganic ion exchangers. Elsevier, Amsterdam

An J, Kang D, Tran K, Kim M, Lim T, Tran T (2012) Recovery of lithium from Uyuni salar brine. Hydrometallurgy 117–118:64–70

Bohnke O (2008) The fast lithium-ion conducting oxides $Li_{3x}La_{2/3-x}TiO_3$ from fundamentals to application. Solid State Ionics 179(1–6):9–15

Certificate of Analysis (1991) Standard reference material. Instrument sensitivity standard for X-ray powder diffraction. Nat Inst of Standards and Technology, Gaithersburg

Chitrakar R, Makita Y, Ooi K, Sonoda A (2014) Lithium recovery from salt lake brine by H_2TiO_3. Dalton Trans 43(23):8933–8939

Cho N, Chang S, Sung H (1997) Synthesis and crystal structure refinement of $LiMn_{(2-d)}Ti_{(d)}O_4$. RIST Yongu Nonmun 11:622–628

Chung K, Lee J, Lee H (2014) Lithium recovery device using separator reservoir, lithium recovery method and lithium adsorption/desorption system using the same. US; 8741150

Chung K, Ryu T, Kim B, Ryu J (2017) Porous manganese oxide absorbent for lithium having spinel type structure and a method of manufacturing the same. US; 8926874

Diebold U (2003) The surface science of titanium dioxide. Surf Sci Rep 48(5–8):53–229

Dzyazko YS, Belyakov VN, Vasilyuk SL, Stefanyak NV (2006) Anion-exchange properties of composite ceramic membranes containing hydrated zirconium dioxide. Russ J Appl Chem 79(5):769–773

Dzyazko YS, Rudenko AS, Yukhin YM, Palchik AV, Belyakov VN (2014a) Modification of ceramic membranes with inorganic sorbents. Application to electrodialytic recovery of Cr(VI) anions from multicomponent solution. Desalination 342:52–60

Dzyazko YS, Volfkovich YM, Sosenkin VE, Nikolskaya NF, Gomza YP (2014b) Composite inorganic membranes containing nanoparticles of hydrated zirconium dioxide for electrodialytic separation. Nanoscale Res: Let 9:271. https://doi.org/10.1186/1556-276X-9-271

Dzyazko YS, Rozhdestvenskaya LM, Zmievskii YG, Vilenskii AI, Myronchuk VG, Kornienko LV, Vasilyuk SL, Tsyba NN (2015) Organic-inorganic materials containing nanoparticles of zirconium hydrophosphate for baromembrane separation. Nanoscale Res Let 10:64. https://doi.org/10.1186/s11671-015-0758-x

Dzyazko YS, Rozhdestvenska LM, Vasilyuk SL, Kudelko KO, Belyakov VN (2017) Composite membranes containing nanoparticles of inorganic ion exchangers for electrodialytic desalination of glycerol. Nanoscale Res Lett 12(1):438. https://doi.org/10.1186/s11671-017-2208-4

Epstein J, Feist E, Zmora J, Marcus Y (1981) Extraction of lithium from the dead sea. Hydrometallurgy 6(3–4):269–275

Gao D, Guo Y, Yu X, Wang S, Deng T (2016) Extracting lithium from the high concentration ratio of magnesium and lithium brine using imidazolium-based ionic liquids with varying alkyl chain lengths. J Chem Eng Jpn 49(2):104–110

Gregg S, Sing K (1982) Adsorption, surface area and porosity. Academic Press, London

Hamzaoui A, M'nif A, Hammi H, Rokbani R (2003) Contribution to the lithium recovery from brine. Desalination 158(1–3):221–224

Heidari N, Momeni P (2017) Selective adsorption of lithium ions from Urmia Lake onto aluminum hydroxide. Environ Earth Sci. https://doi.org/10.1007/s12665-017-6885-1

Helfferich F (1995) Ion exchange. Dover Publications, New York

Hong JG, Chen Y (2015) Evaluation of electrochemical properties and reverse electrodialysis performance for porous cation exchange membranes with sulfate-functionalized iron oxide. J Membr Sci 473:210–217

Hong H, Park I, Ryu T, Ryu J, Kim B, Chung K (2013) Granulation of $Li_{1.33}Mn_{1.67}O_4$ (LMO) through the use of cross-linked chitosan for the effective recovery of L^{i+} from seawater. Chem Eng J 234:16–22

Hong H, Park I, Ryu J, Ryu T, Kim B, Chung K (2015) Immobilization of hydrogen manganese oxide (HMO) on alpha-alumina bead (AAB) to effective recovery of L^{i+} from seawater. Chem Eng J 271:71–78

Hong HJ, Ryu T, Park I-S, Kim M, Shin J, Kim B-G, Chung K-S (2018) Highly porous and surface-expanded spinel hydrogen manganese oxide (HMO)/Al_2O_3 composite for effective lithium (Li) recovery from seawater Chem. Eng J. 337:455–461

Hoshino T (2015) Innovative lithium recovery technique from seawater by using world-first dialysis with a lithium ionic superconductor. Desalination 359:59–63

Huang Z-Q, Zheng F, Zhang Z, Xu H-T, Zhou K-M (2012) The performance of the PVDF-Fe_3O_4 ultrafiltration membrane and the effect of a parallel magnetic field used during the membrane formation. Desalination 292:64–72

Jiang J (2012) Synthesis and research of lithium manganese titanium oxide. Adv Mater Res 549:466–469

Kam S, Park J, Lee M (2015) Adsorption characteristics of lithium ions from aqueous solution using a novel adsorbent SAN-LMO beads. J Environ Sci Int 24(5):641–646

Kim J, Nielsen UG, Grey CP (2008) Local environments and lithium adsorption on the iron oxyhydroxides lepidocrocite (γ-FeOOH) and goethite (α-FeOOH): a 2H and 7Li solid-state MAS NMR study. J Am Chem Soc 130(4):1285–1295

Kudelko K, Maltseva T, Belyakov V (2011) Adsorption and mobility of Cu(II), Cd(II), Pb(II) ions adsorbed on (hydr)oxide polymer sorbents $M_xO_y{\cdot}nH_2O$, M = Zr (IV), Ti(IV), Sn (IV), Mn(IV). Desalin Water Treat 35(1–3):295–299

Lambert P, Harrison M, Edwards P (1988) Magnetism and superconductivity in the spinel system $Li_{1-x}M_xTi_2O_4$ ($M = Mn^{2+}$, Mg^{2+}). J Solid State Chem 75(2):332–346

Mal'tseva TV, Yatsenko TV, Kudelko EO, Belyakov VN (2011) The effect of introduction of manganese hydroxide and hydrated aluminum oxide on the pore structure and surface charge of Zr(IV), Ti(IV), and Sn(IV) oxyhydrates. Russ J Appl Chem 84(5):726–731

Martı-Calatayud MC, Garcıa-Gabaldon M, Perez-Herranz V, Salesb S, Mestre S (2015) Ceramic anion-exchange membranes based on

microporous supports infiltrated with hydrated zirconium dioxide. RSC Adv 5:46348–46358

Miyamoto Y, Kuroda Y, Uematsu T, Oshikawa H, Shibata N, Ikuhara Y et al (2015) Synthesis of ultrasmall Li–Mn spinel oxides exhibiting unusual ion exchange, electrochemical and catalytic properties. Sci Rep. https://doi.org/10.1038/srep15011

Mora-Gómez J, García-Gabaldón M, Martí-Calatayud MC, Mestre S, Pérez-Herranz V (2017) Anion transport through ceramic electrodialysis membranes made with hydrated cerium dioxide. J Am Ceran Soc 100(9):4180–4189

Myronchuk VG, Dzyazko YS, Zmievskii YG et al (2016) Organic–inorganic membranes for filtration of corn distillery. Acta Period Technol 47:153–165

Ooi K, Miyai Y, Katoh S (1986) Recovery of lithium from seawater by manganese oxide adsorbent. Sep Sci Technol 21(8):755–766

Pang R, Li X, Li J, Lu Z, Sun X, Wang L (2014) Preparation and characterization of ZrO_2/PES hybrid ultrafiltration membrane with uniform ZrO_2 nanoparticles. Desalination 332:60–66

Park H, Singhal N, Jho E (2015) Lithium sorption properties of HMnO in seawater and wastewater. Water Res 87:320–327

Scherrer P (1918) Bestimmung der Grosse und der Inneren Struktur von Kolloidteilchen Mittels Rontgenstrahlen. Nachrichten von der Gesellschaft der Wissenschaften, Gottingen. Math Phys Kl 2:98–100

Shi X, Zhang Z, Zhou D, Zhang L, Chen B, Yu L (2013) Synthesis of L^{i+} adsorbent (H_2TiO_3) and its adsorption properties. Trans. Nonferr. Metals Soc. China 23(1):253–259

Swain B (2016) Separation and purification of lithium by solvent extraction and supported liquid membrane, analysis of their mechanism: a review. J Chem Technol Biotechnol 91(10):2549–2562

Tretyak M, Rozhdesvenska L, Belyakov V (2013) Inorganic ion exchange materials based on hydrated titanium dioxide as promising ionites for lithium recovery. Ukr Chem J 79(3):15–20

Umeno A, Miyai Y, Takagi N, Chitrakar R, Sakane K, Ooi K (2002) Preparation and adsorptive properties of membrane-type adsorbents for lithium recovery from seawater. Ind Eng Chem Res 41(17):4281–4287

Xiao J, Sun S, Song X, Li P, Yu J (2015) Lithium ion recovery from brine using granulated polyacrylamide–MnO_2 ion-sieve. Chem Eng J 279:659–666

Zhang C-P, Gu P, Zhao J, Zhang D, Deng Y (2009) Research on the treatment of liquid waste containing cesium by an adsorption–microfiltration process with potassium zinc hexacyanoferrate. J Hazard Mater 167(1–3):1057–1062

Zhang Q, Li S, Sun S, Yin X, Yu J (2010) Lithium selective adsorption on low-dimensional titania nanoribbons. Chem Eng Sci 65(1):165–168